Defining α-synuclein species responsible for Parkinson's disease phenotypes in mice

Received for publication, January 25, 2019, and in revised form, May 22, 2019 Published, Papers in Press, May 29, 2019, DOI 10.1074/jbc.RA119.007743

Jessica M. Froula[‡1], Marta Castellana-Cruz[§1,2], Nadia M. Anabtawi[‡], José D. Camino[¶], Serene W. Chen[§], Drake R. Thrasher[‡], Jennifer Freire[‡], Allen A. Yazdi[‡], Sheila Fleming[‖], Christopher M. Dobson[§2], Janet R. Kumita[§2], Nunilo Cremades[¶3], and Laura A. Volpicelli-Daley[‡4]

From the[‡]Department of Neurology, Center for Neurodegeneration and Experimental Therapeutics, University of Alabama at Birmingham, Birmingham, Alabama 35294, the [¶]Institute for Biocomputation and Physics of Complex Systems (BIFI)–Joint Unit BIFI–IQFR (CSIC), University of Zaragoza, Zaragoza 50018, Spain, the [§]Centre for Misfolding Diseases, Department of Chemistry, University of Cambridge, Cambridge CB2 1EW, United Kingdom, and the [‖]Department of Pharmaceutical Sciences, Northeast Ohio Medical University, Rootstown, Ohio 44272

Edited by Paul E. Fraser

Parkinson's disease (PD) is a neurodegenerative disorder characterized by fibrillar neuronal inclusions composed of aggregated α-synuclein (α-syn). These inclusions are associated with behavioral and pathological PD phenotypes. One strategy for therapeutic interventions is to prevent the formation of these inclusions to halt disease progression. α-Synuclein exists in multiple structural forms, including disordered, nonamyloid oligomers, ordered amyloid oligomers, and fibrils. It is critical to understand which conformers contribute to specific PD phenotypes. Here, we utilized a mouse model to explore the pathological effects of stable β-amyloid–sheet oligomers compared with those of fibrillar α-synuclein. We biophysically characterized these species with transmission EM, atomic-force microscopy, CD spectroscopy, FTIR spectroscopy, analytical ultracentrifugation, and thioflavin T assays. We then injected these different α-synuclein forms into the mouse striatum to determine their ability to induce PD-related phenotypes. We found that β-sheet oligomers produce a small but significant loss of dopamine neurons in the substantia nigra pars compacta (SNc). Injection of small β-sheet fibril fragments, however, produced the most robust phenotypes, including reduction of striatal dopamine terminals, SNc loss of dopamine neurons, and motor-behavior defects. We conclude that although the β-sheet oligomers cause some toxicity, the potent effects of the short fibrillar fragments can be attributed to their ability to recruit monomeric α-synuclein and spread *in vivo* and hence contribute to the development of PD-like phenotypes. These results suggest that strategies to reduce the formation and propagation of β-sheet fibrillar species could be an important route for therapeutic intervention in PD and related disorders.

This work was supported in part by the Michael J. Fox Foundation (to L. V.-D. and N. C.) and Grant P50NS108675 (Alabama Udall Center). The authors declare that they have no conflicts of interest with the contents of this article.
This article was selected as one of our Editors' Picks.
This article contains Figs. S1–S5.
[1] Both authors contributed equally to this work.
[2] Supported by the Cambridge Centre for Misfolding Disease.
[3] To whom correspondence may be addressed. Tel.: 34-876555415; E-mail: ncc@unizar.es.
[4] To whom correspondence may be addressed. Tel.: 205-996-7695; E-mail: lvolpicellidaley@uabmc.edu.

Multiple neurodegenerative diseases are characterized by amyloid inclusions that are formed by the assembly of monomeric proteins into oligomeric intermediates that then grow to form protofilaments, and eventually fibrils (1). In Parkinson's disease (PD),[5] these inclusions are referred to as Lewy bodies and Lewy neurites and are composed primarily of α-synuclein (2), but they also include other proteins such as p62 and ubiquitin (3). They develop from the nucleated polymerization of endogenous α-synuclein that is then thought to spread within neurons and to propagate to interconnected neuronal networks in a spatially and temporally predictable manner (4, 5). The role of α-synuclein in neurodegeneration and in generating symptoms in PD is not yet completely clear and is an area of active research. It is important to note that neurodegeneration is likely to be caused by a combination of factors in addition to α-synuclein inclusion formation such as impaired proteostasis, mitochondrial dysfunction, and activation of inflammation. On the basis of data that support the cell–to–cell spreading of α-synuclein aggregates, however, therapeutic strategies such as immunotherapy are in development in the hope of blocking the invasion of pathogenic α-synuclein species into additional brain regions and hence slowing the progression of PD (6).

Preventing the progression of α-synuclein inclusion formation, however, requires precise definitions of the species that are more highly toxic and those that are capable of promoting the formation of new aggregates by recruiting endogenous monomeric α-synuclein. Assemblies of structurally diverse oligomers and fibrils have varying degrees of pathogenicity (7–9). In a cellular environment, monomeric α-synuclein interacts with membranes and adopts an α-helical, tetrameric conformation (10–12). Monomeric α-synuclein can also assemble into fibrils in an array of heterogeneous oligomeric species that are often transient in nature. Recently, methods have been developed to produce and stabilize oligomers of α-synuclein (7, 13), enabling

[5] The abbreviations used are: PD, Parkinson's disease; AUC, analytical ultracentrifugation; AFM, atomic-force microscopy; PFA, paraformaldehyde; ThioT, thioflavin T; TEM, transmission electron microscopy; ANOVA, analysis of variance; DAT, dopamine transporter; TH, tyrosine hydroxylase; SNc, substantia nigra pars compacta; p-α-synuclein, phosphorylated α-synuclein; O, oligomer; F-L, F-long; F-M, F-Mix; F-S, F-short; OC, omyloid fibril antibody.

these to be extensively characterized. One particularly well-defined type of α-synuclein oligomeric species is composed of ~15–30 protein molecules, adopts a spherical appearance, and contains a rudimentary β-sheet structural core with very limited capability of binding the amyloid-specific dye thioflavin T (ThioT) and of elongating and recruiting new α-synuclein molecules. Addition of these oligomers to cells in culture disrupts membranes, generates reactive oxygen species, increases cytosolic calcium, and increases cell death (7, 13, 14). In contrast, the typical fibrillar forms of α-synuclein show the general amyloid features, including the ability to bind ThioT, the presence of a cross-β core structure, and an elongated filamentous morphology of 10–15 nm diameter. Exposure of neurons to extracellular α-synuclein fibrils induces intracellular endogenous α-synuclein to form inclusions that are morphologically and biochemically similar to those found in diseased brains; they form dense Lewy body-like aggregates in the soma, thread-like Lewy neurites in the neuropil, are insoluble in nonionic detergents, are primarily composed of fibrillar aggregates, and are phosphorylated, ubiquitinated, and proteinase K–resistant (4, 5, 15, 16). Inclusion formation leads to loss of dopaminergic neurons in the SNc with associated motor dysfunctional phenotypes, recapitulating the core features of PD. It has been shown that extensive sonication of α-synuclein fibrils increases the abundance of inclusions (17, 18). Such fragmentation, however, can generate a heterogeneous ensemble of species, including oligomers as well as short and long fibrillar fragments, which likely contributes to the current variability of observed phenotypes in the pre-formed fibril mouse model (19). More precise biophysical characterization combined with *in vivo* experiments is required to define which species contribute more strongly to the neuropathological and neurodegenerative phenotypes.

Here, we produce, isolate, and define reproducible conformers of mouse α-synuclein and monitor the neuropathological and neurodegenerative outcomes in mice injected with different well-defined forms of the protein, namely monomers, stable kinetically-trapped β-sheet oligomers, and fibril fragments. Unilateral injection of the β-sheet oligomers causes a slight but significant loss of dopamine neurons in the SNc, but it does not induce inclusion formation or produce defects in motor behavior; these findings can be attributable to the inability of these oligomers to grow by addition of the monomeric protein. The injections of preparations of short fibrils (70 nm), however, result in the formation of inclusions, the loss of dopamine terminals in the striatum, dopaminergic neurons in the SNc, and motor-behavior defects.

Results

Biophysical and morphological characterization of α-synuclein conformers

To determine the capacity of different structural forms of α-synuclein in the mouse brain to induce PD-related phenotypes, we used recombinant mouse α-synuclein protein for the preparations of the different forms given the lower efficiency of seeding when using cross-species (*i.e.* human) α-synuclein forms (see Fig. 3) (20). We first characterized the stability and structural features of oligomers and fibrils. α-Synuclein fibrils were generated by shaking monomeric α-synuclein for 7 days at 37 °C, and the resulting structures shown by transmission EM (TEM) and atomic-force microscopy (AFM) indicated a long, filamentous structure as observed previously ("F-long, F-L") with an average length of 266 ± 0.5 nm (Fig. 1, *A–D*). Shorter fibrils were then generated by sonication reducing the average length to 120 ± 4.0 nm; these fragments still, however, varied in length from 40 to 225 nm ("F-Mix, F-M") (Fig. 1, *E–H*). Samples enriched in shorter fragments were generated by passing the solution of F-M through a 0.22-μm filter (21, 22), resulting in an average length of 70 ± 3.3 nm and a more homogeneous distribution of 40–125 nm ("F-short, "F-S) (Fig. 1, *I–L*). Stabilized oligomeric species were generated using the procedure described previously for the human variant of the protein (7, 14); these oligomers were observed in TEM and AFM images to have a spherical morphology that was similar to that observed for oligomers generated by human α-synuclein. Their size was more uniform than that of the fibrillar samples, with an average length of 54 ± 0.7 nm and a range of 40–70 nm (Fig. 1, *M–P*). To confirm that the procedures used to generate the oligomers and fibrils did not cause degradation of α-synuclein, oligomer, F-L, F-M, and F-S were incubated with urea to dissociate the fibrils and oligomers into monomers. α-Synuclein was identified using SDS-PAGE, and bands were visualized using either "instant blue" or silver stain. Protein remains unaltered in all the protein samples, except for some minor monomer degradation that occurred in the oligomeric samples with minimal consequences for the study (Fig. S1).

Indeed, the stable, purified oligomers generated by mouse α-synuclein show identical morphological and structural features as the previously reported oligomers of human α-synuclein (Fig. 2*A*) (7). As shown previously for human oligomers, analytical ultracentrifugation (AUC) revealed that mouse oligomers showed two main distributions: one centered at 10S corresponding to a population of oligomers composed of an average of 18 α-synuclein molecules (260 kDa), and the other at 15S, corresponding to oligomers composed of an average of 29 α-synuclein molecules (420 kDa) (Fig. 2*A*), and similar to the size distribution of human oligomers. Also similar to the previously characterized human oligomers, mouse oligomers showed an intermediate structure between the disordered monomer and the β-sheet–rich amyloid fibrils, with an average of 30% of β-sheet structure (F-L, F-M, and F-S show ~60–65%) according to Fourier transform IR (FTIR) and far-UV circular dichroism (CD) spectroscopy analysis (Fig. 2, *B* and *C*) (7, 13). They also showed marginal ability to bind ThioT molecules (Fig. 2*D*), unlike F-L, F-M, and F-S, which showed similar ThioT binding. In addition, the FTIR data also showed a marked difference between the oligomers and the fibrils, whereas the spectra of the fibrils contained an absorbance peak at 1620 cm^{-1} and no absorbance peak at 1695 cm^{-1}, characteristic of a parallel β-sheet configuration; the spectra of the oligomers clearly showed both peaks demonstrating an antiparallel β-sheet arrangement. An antiparallel conformation for stabilized oligomers and parallel conformation for fibrils has previously been

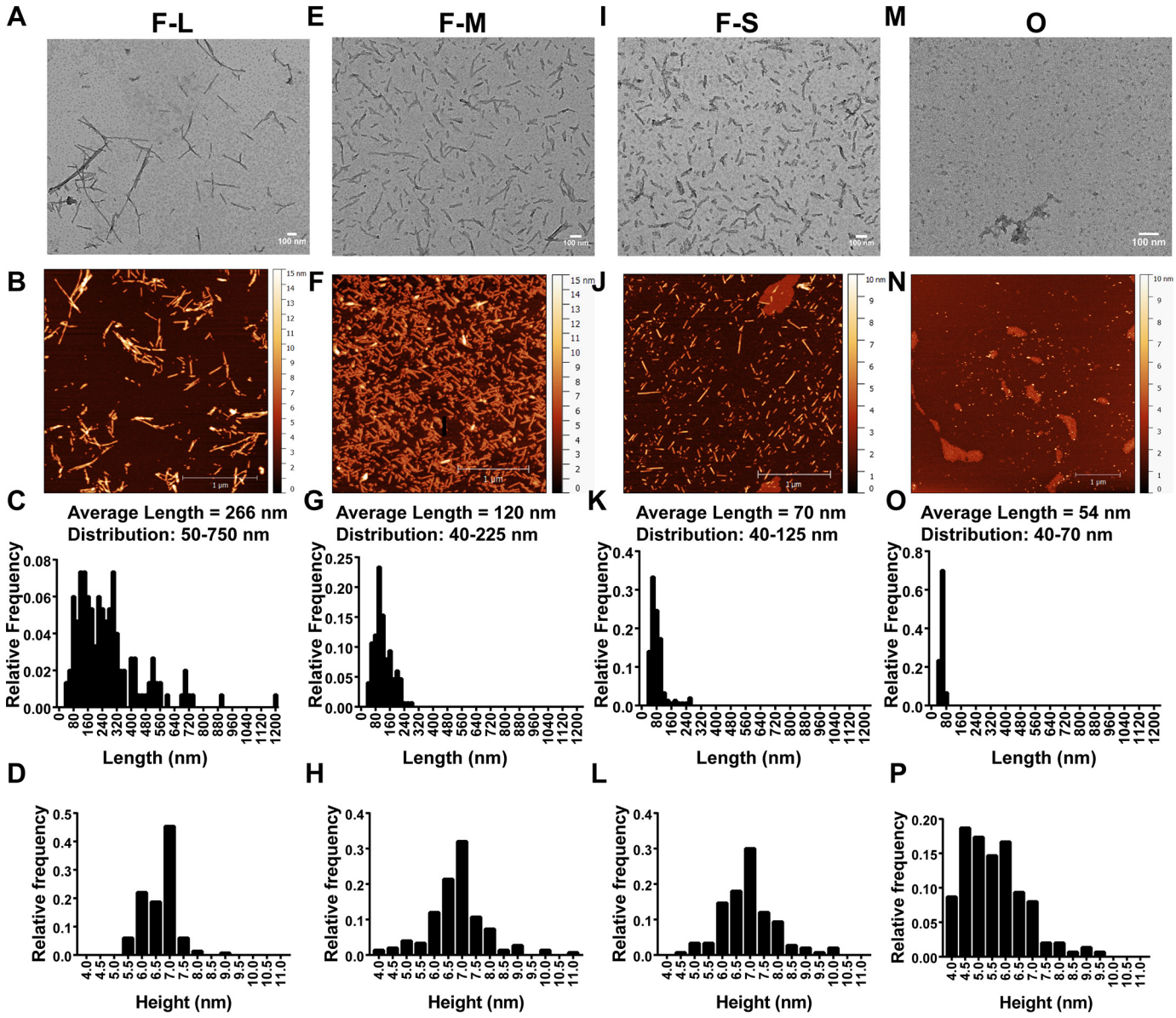

Figure 1. Morphological characterization of the mouse α-synuclein species used in the *in vivo* mouse studies. TEM and AFM images of fibrils (F-L) (*A* and *B*), sonicated fibrils (F-M) (*E* and *F*), sonicated fibrils enriched in short fragments (F-S) (*I* and *J*), and O (*M* and *N*). *C–P,* AFM was used to quantify the length and height of each species shown in the histograms.

observed for human α-synuclein and other amyloidogenic proteins and peptides, such as β-amyloid (23, 24), and the acquisition of the antiparallel β-sheet arrangement has been associated with a lower structural stability and a significantly reduced efficiency in elongation and seeding (7, 25). Indeed, the stable oligomeric species (O) of α-synuclein appear to be trapped species that need to dissociate and reassemble into species with parallel β-sheet structure to readily assemble into fibrils. Antibodies have been generated that recognize toxic conformations of proteins implicated in neurodegeneration (26, 27). The A11 antibodies selectively recognize potentially toxic conformations of proteins implicated in neurodegeneration, particularly pre-fibrillar oligomers, whereas the amyloid fibril OC antibody recognizes fibrils. Dot-blots using these antibodies showed that, as expected, OC recognized FL, FM, and FS. A11 recognized the oligomer preparation but also recognized the sonicated fibrils. A11, however, did not recognize the long fibrils (Fig. S2). These data indicate that the process of fragmenting longer fibrils can produce toxic oligomers, as shown previously (13).

Seeding efficiency of fibrils and oligomers in vitro and in neurons

We first wanted to assess the degree of compatibility between human and mouse α-synuclein in *in vitro* seeding reactions (Fig. 3*A*). Mouse and human fibrils (5 μM) were combined with 100 μM mouse α-synuclein monomer, and the formation of ThioT-positive amyloid fibrils was measured over time. Mouse fibrils seeded the formation of ThioT-positive amyloid fibrils from mouse α-synuclein monomer more rapidly than human fibrils, as shown previously (20). Interestingly, the initial rate of seeding using fibrils and monomers of human α-synuclein pro-

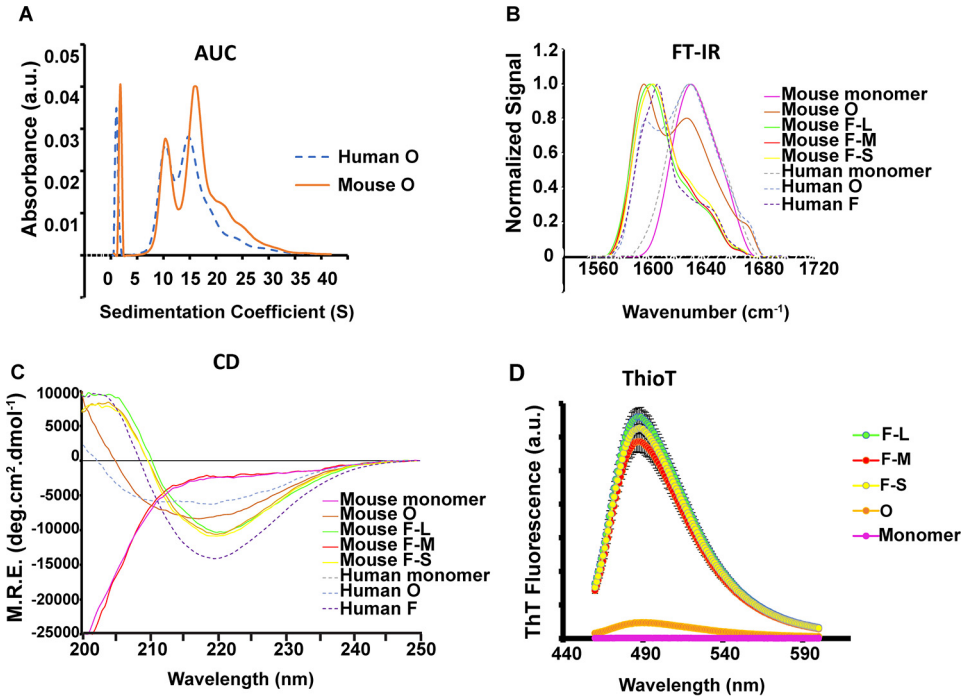

Figure 2. Structural characterization of α-synuclein species used in the *in vivo* mouse studies. *A,* absorbance unit (*a.u.*) sedimentation velocity measurement of human (*blue dashed line*) and mouse oligomers (*orange line*) shows 10S and 15S species. *B,* FTIR spectra show that F-L, F-M, and F-S species are primarily composed of parallel β-sheets (band at 1620–1630) and that the oligomeric (mouse and human) species are primarily antiparallel (band at 1620–1630 cm^{-1} and shoulder at 1695 cm^{-1}). The mouse and human oligomers have β-sheet structures of about 40 and 65%, respectively. *C,* CD shows that β-sheet content of oligomers (mouse and human) are intermediate between monomer and fibrils. *M.R.E.*, mean residue ellipticity. *D,* ThioT binding shows that the fibrils adopt an amyloid conformation; the oligomers show limited ThioT binding, and the monomer shows no ThioT binding.

tein was slower than that observed for mouse α-synuclein and was significantly slower when mouse α-synuclein fibrils were used to seed solutions of human α-synuclein monomers. Thus, the seeding efficiency was found to be higher when the species of α-synuclein seeds matches that of the free monomers; therefore, in the *in vivo* seeding studies that involve endogenous expression of mouse α-synuclein, it is recommended to use fibrillar seeds generated from mouse α-synuclein.

Using mouse protein, the ability of the oligomers and the different sizes of fibrils to seed formation of ThioT-positive amyloid fibrils were also determined (Fig. 3*B*). Seeding with the oligomers was highly inefficient and produced negligible fibril formation over time, a finding consistent with previous data for the human protein showing that these oligomers are trapped in a conformation distinct from that of the fibrillar species that is unable to efficiently elongate (7). In contrast, all the fibrillar samples used in this study were highly efficient in the seeding reactions.

To examine the ability of different α-synuclein fibrils to seed inclusion formation in neurons, 0.05 μM concentrations of monomeric, O, F-L, F-M, or F-S were added to WT primary hippocampal neurons, and the abundance of phosphorylated α-synuclein, a marker of pathological α-synuclein inclusion formation in cells, was measured (Fig. 3, *C* and *D*) (28). Neither monomeric nor oligomeric α-synuclein was found to produce p-α-synuclein inclusions, a result consistent with the finding that these forms of α-synuclein were not able to seed fibril formation *in vitro*. Immunofluorescence appeared diffuse and faint in experiments with both forms of α-synuclein. F-M and F-S produced similar quantities of inclusions, the majority of which appeared as bright and thread-like structures similar to Lewy neurites found in synucleinopathy brains. In contrast, a small quantity of p-α-synuclein was visible in neurons exposed to the long fibrils, which is significantly lower compared with the levels observed in neurons exposed to fragmented fibrils (Fig. 3, *C* and *D*). To determine whether fibrils are more efficient at inducing α-synuclein inclusion formation because they are more efficiently internalized than oligomers, an internalization assay using α-synuclein labeled with Alexa488 was performed (29). This assay utilizes trypan blue to quench the fluorescence of extracellular α-synuclein conformers to distinguish extracellular from intracellular α-synuclein. In addition, when trypan blue binds to proteins on the membrane surface, it fluoresces when excited at 560 nm, allowing visualization of soma and neurites. Both short Alexa488-labeled α-synuclein fibrils (F-S) and O were internalized, whereas unsonicated fibrils showed minimal internalization, as demonstrated previously (Fig. 3*E*) (29). Surprisingly, oligomers showed significantly increased internalization compared with fibrils, indicating that the efficiency of fibril uptake does not account for robust inclusion formation. Table 1 summarizes the structural and morphological features of all the α-synuclein species used in this study.

Formation of inclusions in the brain by fibrils and oligomers

To determine the extent to which the oligomers and the different lengths of fibrils seed the formation of α-synuclein inclusions in the brain, mice received unilateral striatal injections of each species with the mass concentrations in the samples measured immediately after injection. Monomeric α-synuclein was

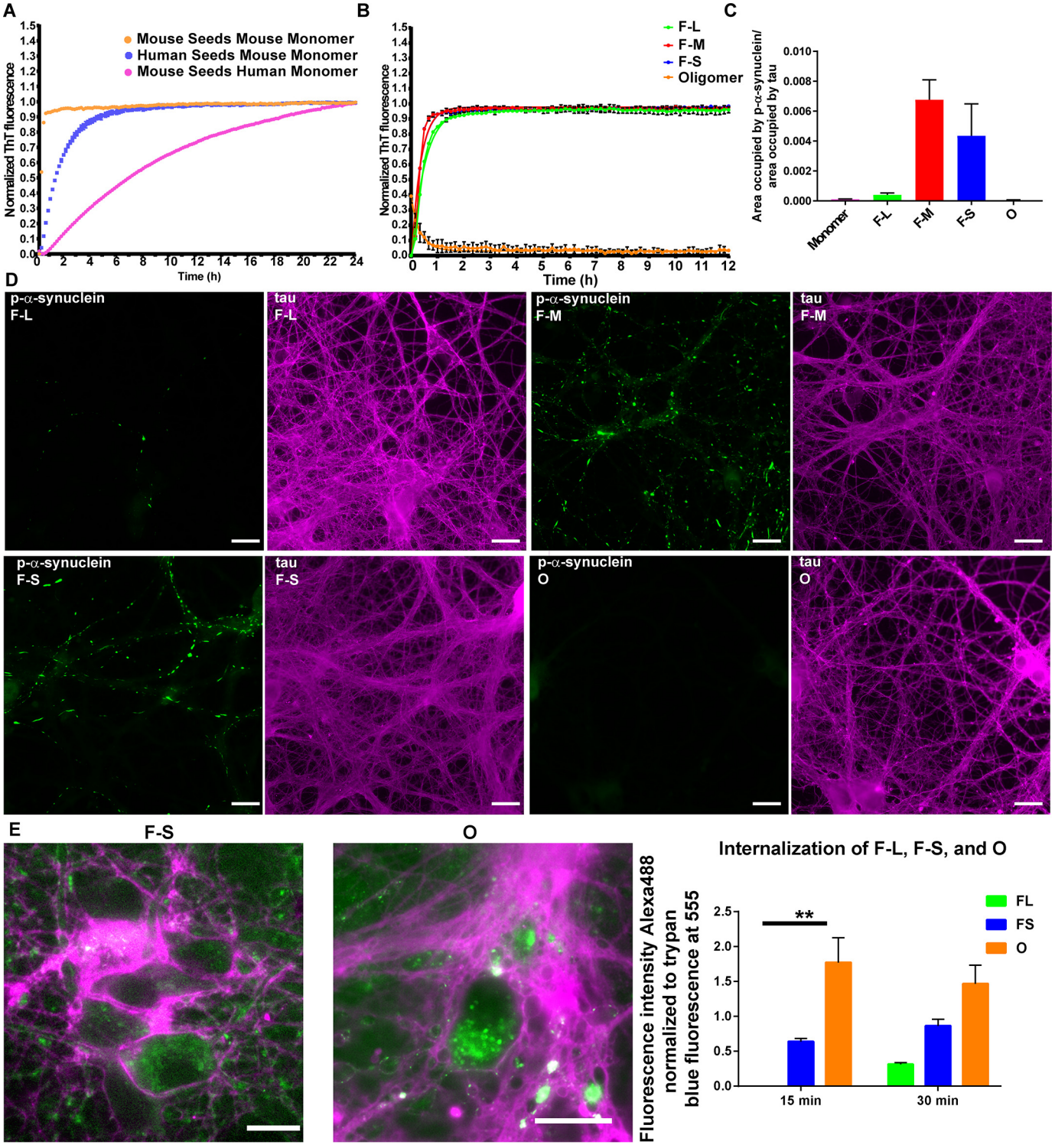

Figure 3. Seeding ability of the difference assembled forms of α-synuclein species *in vitro* and in primary neurons. *A* and *B,* monomer (100 μM) was incubated with 5 μM fibrillar or oligomeric seeds, and the fluorescence of samples incubated with ThioT was quantified over time. *C* and *D,* for the primary hippocampal neurons, 70 nM F-L, F-M, F-S, or oligomers were added to the neurons, and after 7 days, the neurons were fixed, and inclusion formation was visualized using an antibody to p-α-synuclein (*green*). Immunofluorescence for tau (*magenta*) shows the distribution of axons (*scale bar,* 50 mm). ImageJ was used to quantify the percent area occupied by p-α-synuclein fluorescence normalized to the area occupied by tau fluorescence. The data are presented as the mean ± S.E. *E,* primary hippocampal neurons were preincubated with Alexa488-tagged F-L, F-S or O for 30 min at 4 °C to allow binding to the cell surface. The neurons were then incubated for 15 or 30 min at 37 °C to allow internalization. Fluorescence of external α-synuclein–Alexa488 was quenched using trypan blue. Images show representative α-synuclein–Alexa488 fibrils or oligomers. When trypan blue binds to proteins on the cell surface, it fluoresces at 560 nm, which is shown in the images as *magenta* (*scale bar,* 50 μm). The fluorescence intensity of Alexa488 from 10 fields per condition was quantified and normalized to trypan blue immunofluorescence. The internalization experiments were repeated two times. **, $p < 0.01$.

Table 1
Summary of biophysical characteristics of the species of α-synuclein used in this study
NA means not applicable.

Species	Average length	Secondary structure	Configuration	Amyloid	Seeding-competent
	nm				
Monomer	NA	Random coil	NA	No	No
Fibrils	266	60% β-sheet	Parallel	Yes	Yes
Fragmented fibrils (mix, "F-M")	120	60% β-sheet	Parallel	Yes	Yes
Fragmented fibrils (short, "F-S")	70	60% β-sheet	Parallel	Yes	Yes
Oligomers ("O")	54	30% β-sheet	Anti-parallel	No	No

also injected as a control. In the case of the oligomeric samples, the concentration of α-synuclein was determined by absorbance at 280 nm (the extinction coefficient used was 8278 M^{-1} cm^{-1} for oligomers); the fibrillar samples were first dissociated into monomeric units using guanidinium hydrochloride, and the concentration of protein in the sample was then determined (the extinction coefficient used was 7450 M^{-1} cm^{-1}). The concentration of the oligomers was determined to be 300 μM and that of F-L, F-M, and F-S to be 150 μM, although the fibrils were initially prepared using 300 μM α-synuclein. Since this study was initiated, we published a recommendation that fibrils should be freshly made before injections, rather being frozen ,and that the concentration of fibrils should be measured immediately before injection (19). Thus, the concentration of oligomers injected was twice that of the fibrils in terms of monomer equivalents.

The mice were perfused 3 months after injection of the α-synuclein species. Immunohistochemistry was performed using an antibody specific for α-synuclein phosphorylated at serine 129, one of the post-translational modifications of α-synuclein in Lewy neurites and Lewy bodies in synucleinopathy brains (28). In synucleinopathy models, there is very little pSer-129–α-synuclein in neurons from control WT mice. However, exposure of neurons to fibrils produces α-synuclein–abundant inclusions that are highly phosphorylated (5). These fibril-induced inclusions have also been shown in previous studies to be ubiquitin- and p62-positive and are insoluble in detergent (5, 16, 30–32). Importantly, when neurons from α-synuclein knockout mice are exposed to fibrils, the neurons show minimal pSer-129–α-synuclein immunoreactivity (4). In both monomer- and oligomer-injected mice (Fig. 4*A*), immunoreactivity for p-α-synuclein appeared to be diffuse in the cytosol, possibly representing a pool of monomeric α-synuclein protein targeted for degradation (33). Unilateral striatal injections of F-L, F-M, and F-S all resulted in the formation of p-α-synuclein–positive inclusions that produced more intense signals compared with oligomer-injected mice. The inclusions appeared as Lewy neurite-like threads in the neuropil and skein-like inclusions in the soma. The abundance of neurons with inclusions in the soma was measured using a semi-quantitative rating scale (Fig. S3), and the average level within the animals in each group was calculated. Table 2 shows the list of the brain areas containing inclusions along with a ranking based on the quantification process in the different brain areas. The brain areas with the most abundant inclusions included the cortex, amygdala, and striatum. Except for the SNc, which only showed inclusions on the side ipsilateral to the injection, all the brain areas investigated showed bilateral inclusions after unilateral injections of α-synuclein species in the striatum, although the ipsilateral side consistently showed more inclusions than the contralateral side (Fig. 4*C*). The fragmented fibrils (F-M and F-S) produced significantly more inclusions than nonfragmented fibrils (F-L), although there were no significant differences in the abundance of inclusions between F-M- and F-S–injected mice (Fig. 3).

Appearance of p-α-synuclein inclusions in different brain regions at different time points following injections of fibrillar species

The most abundant inclusions appear in the cortex, amygdala, and SNc. These brain regions all project to the striatum (34), suggesting that the aggregates are internalized into the axon terminals, and the resulting inclusions spread within the neuron to the soma. This is consistent with findings that after addition of fibrils to neurons of nontransgenic mice endogenously expressing α-synuclein, inclusions appear first in axons and then at later time points in the soma (4), and is also consistent with the highest concentration of α-synuclein being at the presynaptic terminals (35). To confirm the observation that inclusions appear in brain nuclei that project to the striatum, we co-injected the fibrillar samples with retrotracer beads into the right dorsolateral striatum. Neither the retrotracer beads nor *p*-α-synuclein–positive inclusions had appeared in the SNc (Fig. 5*A*) or amygdala 1 week after injections. In the cortex, however, small fluorescent p-α-synuclein puncta that were co-localized with retrotracer beads were visible. Two weeks after injection, however, *p*-α-synuclein–positive inclusions were visible in the SNc, cortex, and amygdala in the same area as the retrotracer beads. By 4 weeks after injection, p-α-synuclein–positive inclusions were abundant in all three brain regions. These data show that the formation of p-α-synuclein–positive inclusions after injection of fibrils is not apparent until about 1 week after injections and that the cortex is the first area affected.

Loss of dopamine terminals in the striatum and dopamine neurons in the SNc

Unilateral injection of sonicated fibrils into the striatum was previously shown to produce a significant, ~35%, loss of dopaminergic neurons in the SNc relative to mice injected with saline solution (5). The loss occurred 6 months following injection of fibrils, although there were no statistically significant differences in the numbers of tyrosine hydroxylase (TH)–positive dopamine neurons 3 months after injection. Here, we used unbiased stereology to quantify the numbers of TH-positive neurons in the ipsilateral and contralateral SNc of mice

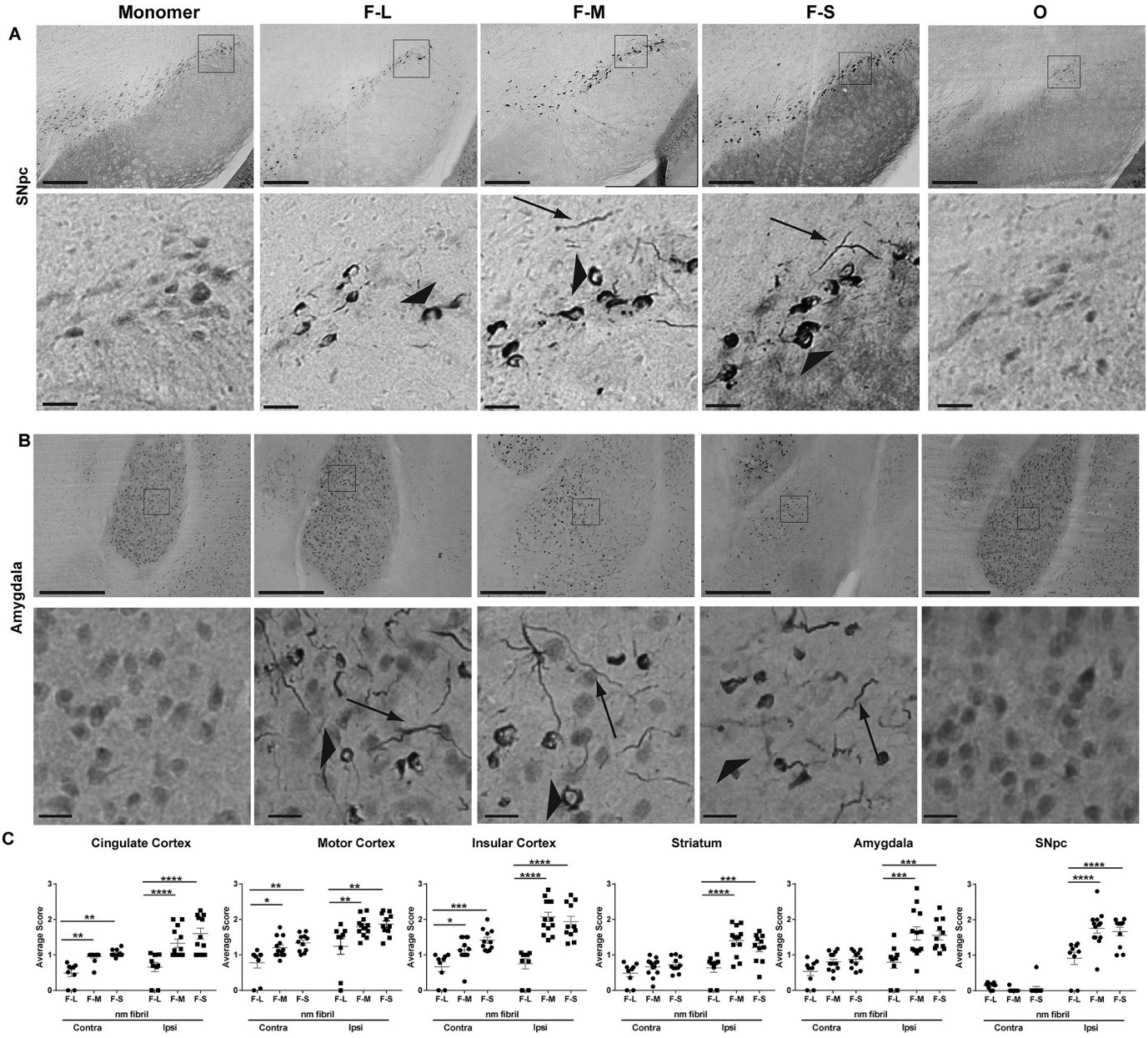

Figure 4. Inclusion formation in the mouse brain after injection of different forms of α-synuclein. C57BL/6J mice received unilateral striatal injections of 2 μl of soluble monomer (300 μM), F-L (150 μM), F-M (150 μM), F-S (150 μM), and O (300 μM). After 3 months, mice were perfused, and immunohistochemistry was performed using an antibody to p-α-synuclein. Representative images from the SNc (*A*) and amygdala (*B*) are shown. *Arrowheads* indicate inclusions in the soma, and *arrows* indicate Lewy neurite-like inclusions. *C,* abundance of inclusions was measured by an investigator blinded to experimental conditions (supporting material 1). Numbers of mice are as follows: monomer (12); F-L (11); F-M (12); F-S (11); and O (15). Data are shown as the mean score ± S.E. and were analyzed using a two-way ANOVA, α-synuclein species/cingulate $F(2,30) = 37.85$, $p < 0.0001$; α-synuclein species/motor cortex $F(2,30) = 7.9$, $p < 0.002$; α-synuclein species/insular cortex $F(2,30) = 22.3$, $p < 0.0001$; α-synuclein species/striatum $F(2,30) = 8.5$, $p < 0.001$; α-synuclein species/amygdala $F(2,30) = 6.6$, $p = 0.004$; α-synuclein species/SNc $F(2,30) = 6.2$, $p < 0.005$. *, $p < 0.05$; **, $p < 0.01$; ***, $p < 0.001$; ****, $p < 0.0001$. *Scale bar,* 100 μm (*top panels*); 20 μm (*bottom panels*).

unilaterally injected with the different α-synuclein species. Three months after injection, only F-S produced a significant, ~30%, loss of dopaminergic neurons compared with monomer-injected mice in the ipsilateral SNc (Fig. 6). The number of dopaminergic neurons on the side ipsilateral to the injection site were significantly reduced relative to the noninjected side (Fig. 6*B*). Oligomers produced a significant reduction in the number of neurons on the side ipsilateral to the injection site relative to the noninjected side. To determine whether dopamine neurons are dying in mice injected with α-synuclein species or whether TH levels are simply being down-regulated, double-labeling immunofluorescence measurements for TH and NeuN (Fig. S4) were performed in the SNc. Compared with mice that received unilateral injections of monomeric α-synuclein, there was a slight, but not statistically significant, reduction in the number of NeuN-positive neurons in the mice that received unilateral injections of F-S. The TH immunofluorescence in the F-S- and O-injected mice appeared beaded compared with monomer-injected mice, suggestive of dying neurons. How-

Table 2
Mice received unilateral striatal injections of F-S and were perfused 3 months later

Immunohistochemistry was performed on brain sections using an antibody to p-α-synuclein. The abundance of inclusions in these brain areas was rated on a scale from 0 to 3 (see Fig. S1), and the brain areas are listed in order of average score. Brains from nine independent mice were scored to obtain the average score.

Brain area	Average p-α-synuclein score–ipsilateral	Average p-α-synuclein score– contralateral
Motor cortex	1.6	1.1
Somatosensory cortex	1.6	1
Insular cortex	1.6	1
SNc	1.6	0
Auditory cortex	1.4	0.9
Lateral orbital cortex	1.3	0.9
Amygdala	1.3	0.6
Ectorhinal cortex	1.3	0.9
Striatum	1.1	0.5
Cingulate cortex	1.0	1.0
Visual cortex	1.0	0.4
Piriform cortex	1.0	0.5
Nucleus accumbens	0.4	0.4
Retrosplenial cortex	0.7	0.3
Subiculum	0.6	0
Hippocampus	0.4	0
Mammillary nucleus	0.5	0.1
Olfactory tubercle	0.2	0
Fimbria	0	0
Cerebellar flocculus	0	0
Colliculus	0	0

ever, there were also TH-positive neurons that appeared healthy. These findings suggest the existence TH-positive dopaminergic and nondopaminergic neuron subtypes in the SNc that resist toxic α-synuclein fibrils.

The loss of dopamine terminals from the striatum was measured by immunofluorescence detection of the dopamine transporter (DAT) (Fig. 6, *C* and *D*). Mice injected with both F-M and F-S showed a significant, ~30%, reduction in DAT-positive dopamine terminals relative to monomer-injected mice. However, only F-M–injected mice showed a statistically significant loss of TH-positive axons in the SNc (Fig. S5). The difference between DAT and TH labeling in the striatum could simply result from technical differences in immunofluorescence labeling or differences between vesicularly-localized DAT *versus* cytosolically-localized TH. Alternatively, the possible interaction between α-synuclein aggregates and DAT may alter the trafficking and localization of this transporter, which could potentially be an interesting line of investigation for the future. In addition, unlike the unilateral loss of dopamine neurons in the SNc, the loss of dopamine terminals in the striatum was bilateral. Thus, smaller fibrils of α-synuclein cause a loss of dopamine neurons and dopamine terminals at 3 months following injections.

Motor-behavior defects caused by fibrils and oligomers

We next determined whether injection of fibrils and the consequent loss of dopaminergic neurons and terminals were associated with defects in motor behavior. After 3 months, only mice that received unilateral injections of F-S showed a significant increase relative to untreated mice in the time needed to descend a pole, a well-established test for "bradykinesia" (Fig. 7) (36). Using the cage hang test, a test of motor strength, it was found that only F-S–injected mice also dropped from the lid of a cage in consistently shorter times compared with control mice, also indicative of motor defects (5). There were no significant differences among any of the groups of treated mice in an open field test for time spent in the center of the field (a measure of "anxiety) or in the speed of movement. A cylinder test modified specifically for mice (37) also showed no differences among the groups in the average numbers of hind limb steps or rears. Injections of short fragments of fibrils therefore show much greater defects in behavioral tests of bradykinesia and motor strength compared with much larger fibrils and toxic but propagation-deficient oligomers.

Discussion

Designing therapeutic strategies to halt the progression and spread of synucleinopathies such as PD requires characterization of the specific forms of α-synuclein that are responsible for given phenotypes, including the formation of inclusions in multiple brain areas, the loss of dopamine terminals, the reduction in the numbers of neurons in the SNc, and the loss of normal motor behavior. In this study, we have used a combination of biophysical, biochemical, and behavioral assays to demonstrate that small aggregates composed primarily of small fragments of α-synuclein fibrils are able to induce typical features of PD when injected into the brains of healthy mice. Such aggregates are able to grow and recruit endogenous monomeric α-synuclein, suggesting that these species are important agents for the spreading of toxicity and disease. By contrast, stable oligomeric aggregates of α-synuclein, which do not undergo elongation, were unable to induce the formation of inclusions by endogenous α-synuclein, to cause loss of dopamine terminals in the striatum, to cause loss of dopamine neurons in the SNc, or to cause deficiencies in motor behavior. The oligomers, however, caused a significant loss of dopamine neurons in the SNc on the side ipsilateral to the injection compared with the contralateral side, a finding consistent with their established cytotoxic nature but lack of seeding potency (7, 14, 38, 39). Considering all the present results together, we demonstrate that other properties, in addition to toxicity, such as the ability of aggregates to seed the formation of new aggregates and to spread between cells, are important for the induction of PD phenotypes in an animal model and that the α-synuclein species that are most efficient in spreading pathology are small fibrillar aggregates, particularly fibrillar oligomers with high-seeding efficiency. Indeed, our results suggest that the ability of aggregated species to recruit monomeric protein molecules and to generate new toxic aggregates is a more important feature than the inherent toxicity of the injected species for the development of PD-related phenotypes (*i.e.* highly-toxic, seeding-deficient oligomers *versus* less toxic and seeding-competent small fibrils). In addition, our results suggest that the major disease-spreading agents consist of seeding-efficient α-synuclein small fibrillar aggregates rather than the possible specific conformers generated from the toxic cascade of events induced by the toxic aggregates and that could be transferred from damaged to healthy cells. Finally, given the potential highly toxic and seeding-competent nature of the fibrillar oligomers generated during the aggregation reaction, in contrast to the seeding-deficient features of the kinetically trapped oligomers used in this study, as well as their high efficiency in enabling cell internalization compared with the fibrillar species, we hypothesize that

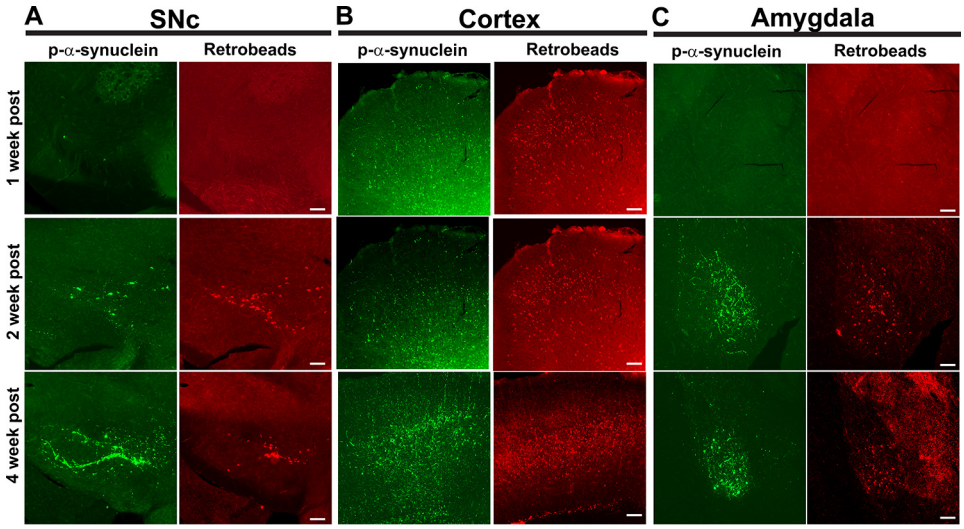

Figure 5. Appearance of p-α-synuclein inclusions in brain areas that project to the striatum. Fibrils and retrotracer beads were co-injected unilaterally into the striatum. After 1 week ($n = 3$), 2 weeks ($n = 3$), or 4 weeks ($n = 3$), mice were perfused, and immunofluorescence to p-α-synuclein (*green*) was performed. The retrotracer beads are shown in *red,* and the merged images include p-α-synuclein, retrotracer beads, and Hoechst (*blue*). Representative images from the SNc, motor cortex, and amygdala are shown.

these species are also likely to be important players in the development and spreading of disease. Indeed, we have recently observed that the interaction of extracellular short fibrillar species with cells results in the generation of on-pathway oligomers that are readily internalized[6] and that could therefore efficiently seed the intracellular formation of new toxic aggregates. Overall, our results highlight the importance of fibrillar aggregates of α-synuclein in the induction of PD-related phenotypes. Future studies to examine the mechanisms by which larger inclusions can fragment within the cell to become new and efficient nuclei for the propagation of α-synuclein inclusions and disease phenotypes will be of great interest, including disaggregation by chaperones or lysosomal proteases (40).

Our results suggest that inhibiting the accumulation of small fibrillar α-synuclein fragments generated either during the process of protein aggregation or by the fragmentation or disaggregation of longer fibrils have the potential to be a therapeutic strategy against PD progression. Indeed, immunotherapy using antibodies raised against α-synuclein are in phase II clinical trials (6). However, antibodies that are not selective for fibrillar α-synuclein also reduce the total concentration of α-synuclein and may have deleterious effects because decreasing levels of α-synuclein impairs dopamine transmission (41, 42). Antibodies that selectively target fibrillar aggregates and reduce their ability to spread from cell–to–cell could therefore reduce the rate of disease propagation. One example is BIIB054, which selectively binds fibrillar α-synuclein (43), and in mouse models of PD, intraperitoneal injections of this antibody inhibited inclusion formation, dopamine neuron loss, and defects in motor behavior.

It has been shown that formation of α-synuclein oligomers *in vivo* by expression of human α-synuclein pathological variants using lentivirus induces loss of dopamine neurons (44). The oligomers used in this study have antiparallel β-sheet structure, whereas the fibrillar structures are parallel, and so they are unable to elongate as they are kinetically trapped. It is likely that oligomers containing a parallel β-sheet structure are transient species involved in the formation of fibrils and are therefore able to elongate and proliferate. In addition, it is also likely that a range of different types of oligomeric species exist *in vivo*, including species bearing post-translational modifications, which are likely to share with the fibrillar species the ability to disrupt membranes and to perturb other cellular processes such mitochondrial function (45, 46).

Overall, our data highlight the importance of precise biophysical definitions of the aggregated forms of α-synuclein that are responsible for the major events of dysfunction related to PD. In this study, injection of the small fibrillar fragments (~70 nm in length) produced p-α-synuclein inclusions, neuronal loss, and motor dysfunction. The fibril preparation, similar to that used in previous studies (5, 30), containing longer fragments (40–225 nm) produced p-α-synuclein inclusions but did not cause significant dopamine neuron loss or behavioral phenotypes at 3 months following injections. This result indicates that fibril preparations enriched for small fragments will produce the most robust phenotypes. Although the fibril model is becoming widely accepted for reproducing PD-like pathology, variability has been reported in obtaining phenotypes that could be caused by heterogeneous fibril preparations with a wide range of fibril sizes.

Although the length of fragments does not substantially influence the seeding of fibril formation *in vitro*, smaller fragments are required for seeding of α-synuclein pathology in neurons and in the brain. This is likely to be because the smaller fragments bind more efficiently to cell-surface receptors such as Lag3, Na^+K^+-ATPase, and heparin sulfate proteoglycans, and only the smaller fragments can be internalized by endocytosis (47–49). Furthermore, smaller fragmented fibrils are the most likely species to be released from neurons and to propagate throughout the brain.

Our study adds to the results of earlier investigations that demonstrated that aggregates consisting solely of α-sy-

[6] N. Cremades, submitted for publication.

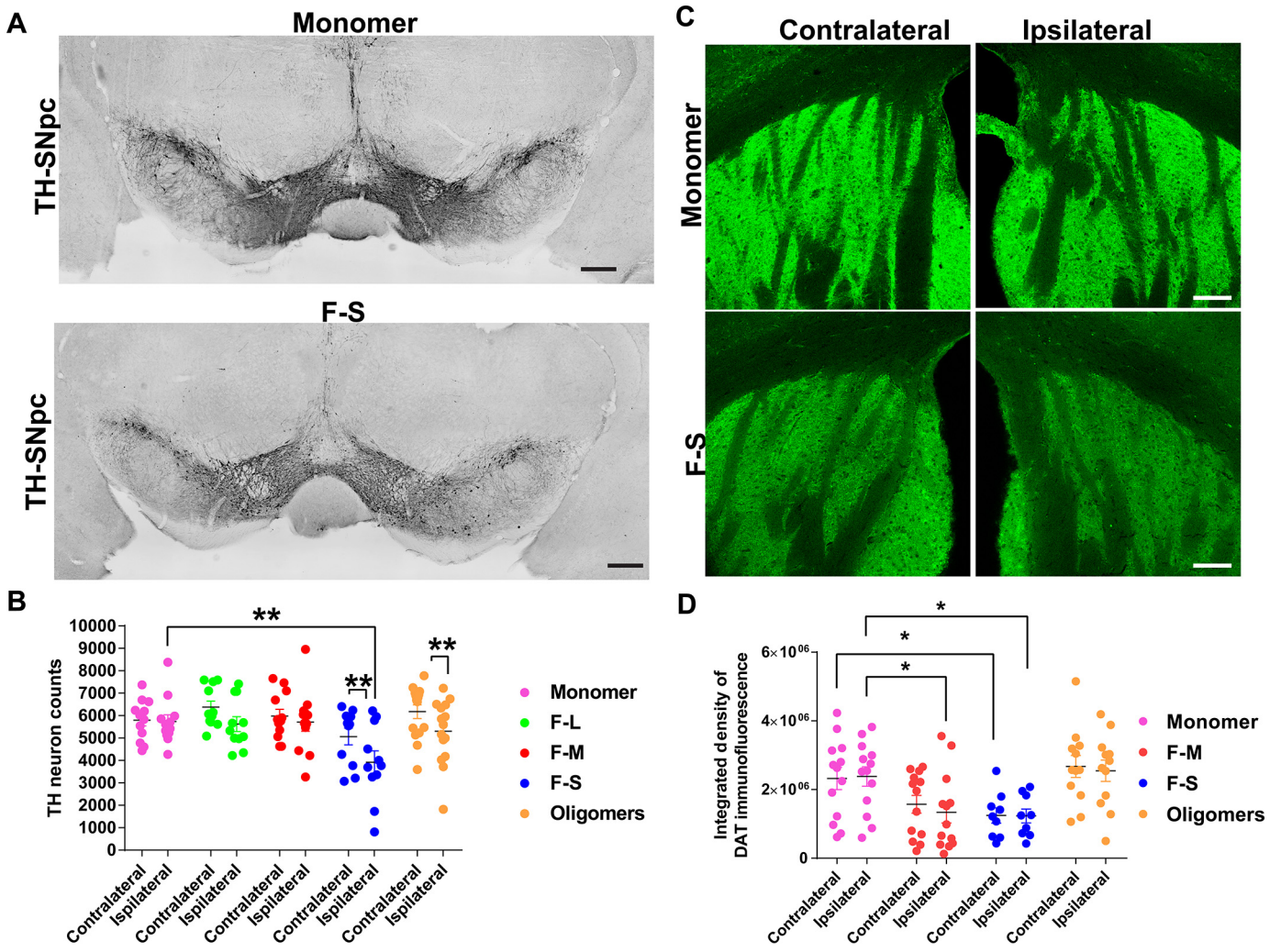

Figure 6. Quantitation of TH-positive neurons in the SNc and DAT terminals in striatum following unilateral striatal injections of different α-synuclein species. C57BL/6J mice received unilateral striatal injections of 2 μl of soluble monomer (300 μM), F-L (150 μM), F-M (150 μM), F-S (150 μM), and O (300 μM). After 3 months, the mice were perfused, and immunostaining was performed. Numbers of mice are as follows: monomer (12); F-L (11); F-M (12); F-S (11); and O (15). *A,* representative images of tyrosine hydroxylase immunohistochemistry in the SNc of monomer- and F-S–injected mice. *B,* unbiased stereology of tyrosine hydroxylase–positive neurons performed by an investigator blinded to experimental conditions. Data are shown as the mean counts ± S.E. and analyzed using a two-way ANOVA, α-synuclein species $F(5,67) = 2.7$, $p = 0.03$. *C,* immunofluorescence performed using an antibody to DAT. Images were captured using confocal microscopy. Representative images of the striatum from monomer and F-S–injected mice are shown. *D,* ImageJ was used to quantify the integrated fluorescence intensity of DAT in the striatum. Data are shown as the mean counts ± S.E. and analyzed using a two-way ANOVA, α-synuclein species $F(3,43) = 5.7$, $p = 0.002$. *, $p < 0.05$; **, $p < 0.01$. *Scale bar,* 100 μm.

nuclein can generate PD phenotypes (5, 16, 30, 31, 50). However, in the future, it will be of great interest to characterize the structural properties of aggregates purified from diseased brains. Interestingly, brain extracts from patients with multiple system atrophy have been reported to be more effective than those from PD brains at inducing α-synuclein inclusion formation and disease spreading when injected into experimental animals (51, 52). α-Synuclein species involved in Lewy body disease may bind receptors in the cortex and limbic regions more readily than do species involved in PD, which may bind more efficiently to receptors in the SNc. Future studies are required to determine how different aggregates contribute to specific disease phenotypes. Overall, our findings indicate that small fibrillar aggregates of α-synuclein are necessary for inducing pathology and spreading, and they suggest that therapeutics should aim to reduce formation and accumulation of such species.

Experimental procedures

Animals

All animal protocols were performed at AAALAC-accredited sites and approved by the University of Alabama at Birmingham Institutional Animal Care and Use Committee. C57BL/6J male mice were obtained from The Jackson Laboratory and housed in groups of no more than five animals per cage. Food and water were accessible 24 h, and animals were kept on a 12-h light/dark cycle.

Preparation of α-synuclein species

α-Synuclein monomer was purified according to previously published protocols (53). The presence of endotoxin was detected using the Pierce LAL chromogenic endotoxin quantitation kit and cleaned using Pierce high-capacity endotoxin removal spin columns. Endotoxin levels were measured to be

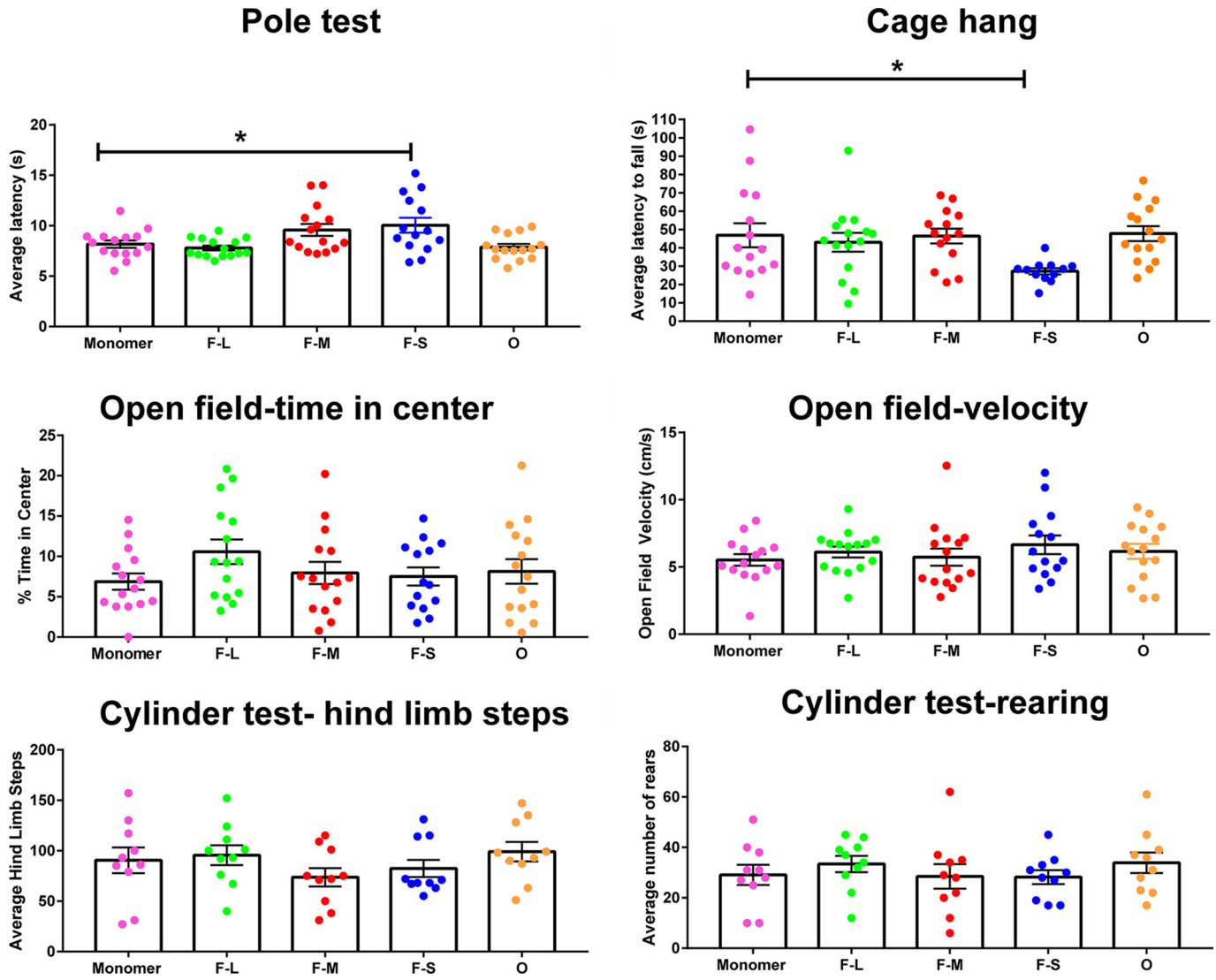

Figure 7. Motor behavior of mice following unilateral striatal injections of different α-synuclein species. C57BL/6J mice received unilateral striatal injections of 2 μl of monomer (300 μM), F-L (150 μM), F-M (150 μM), F-S (150 μM), and O (300 μM). Three months later, mice were subjected to the following behavior tests: open field, pole test, cage hang, and cylinder test (modified for mice). Numbers of mice for pole test, cage hang, and open field are as follows: monomer (12); F-L (11); F-M (12); F-S (11); and O (15). Numbers of mice for cylinder test are as follows: monomer (10); F-L (10); F-M (10); F-S (10); and O (10). The data were analyzed by one-way ANOVA: pole test $F(4,69) = 4.7$, $p = 0.002$; cage hang $F(4,66) = 2.86$, $p = 0.03$; open field/% time center $F(4,69) = 1,1$, $p =$ not significant; open field/velocity $F(4,69) = 0.6$, $p =$ not significant; hind limb steps $F(4,45) = 1.1$, $p =$ not significant; rearing $F(4,45) = 0.5$, $p =$ not significant. *, $p < 0.05$.

less than 0.0113 ng/ml. α-Synuclein fibrils were prepared as published previously (53). Before surgeries, fibrils were sonicated using a ⅛-inch probe tip sonicator (Thermo Fisher Scientific catalog no. FB120110) at 30% power for 30 s total, 1 s on and 1 s off. Short fibrils were isolated using an EMD Millipore Millex0.22-μmfilterunit.Immediatelybeforeinjectionsofmonomeric α-synuclein, α-synuclein protein was spun at 20,000 × *g* at 4 °C. β-Sheet kinetically trapped α-synuclein oligomers were freshly prepared as described previously (7, 13, 14). Briefly, 6 mg of lyophilized protein was resuspended in PBS buffer at a pH of 7.4 and at a concentration of 12 mg·ml^{-1}. The solution was filtered through a 0.22-μm cutoff filter and subsequently incubated at 37 °C for 24 h in stationary mode and without agitation. Small numbers of fibrillar species formed during the incubation were removed by ultracentrifugation for 1 h at 90,000 rpm (using a TLA-120.2 Beckman rotor; 288,000 × *g*). The excess of monomers and small oligomers in the sample was then removed by means of several filtration steps using 100-kDa cutoff membranes, which resulted in the enrichment and concentration of the oligomeric α-synuclein species. The oligomers prepared in this manner have been found to be stable for many days (7). They were shipped from The University of Cambridge, the same day of preparation and injected the day of receipt (1/2 days after preparation) to ensure a stable, characterized conformation.

Biophysical characterization of α-synuclein conformers

A comparative morphological and structural analysis of the different conformers has been performed using a variety of complementary biophysical techniques, and a detailed structural analysis has recently been carried out with oligomers of human α-synuclein using both cryo-EM and solution and solid-

state NMR spectroscopy (7, 14). TEM images were obtained using a Philips CEM100 transmission electron microscope (CAIC, University of Cambridge, UK). The samples were applied to Formvar carbon-coated nickel grids, washed with double-distilled H_2O, and negatively stained with 2% (w/v) uranyl acetate. AFM images were acquired using tapping mode in a Multimode 8 atomic force microscope (Bruker, Billerica, MA). The different α-synuclein species (0.1–1 μM, 10 μl) were applied onto a layer of freshly cleaved mica and allowed to air-dry. The samples were washed with water to remove any salts and dried again before imaging. Images were processed with Gwyddion open source software (http://www.gwyddion.net).[7] Sedimentation velocity measurements using AUC were carried out at 20 °C at 38,000–43,000 rpm (106,750–136,680 × *g*) by using a Beckman-Coulter Optima XL-I analytical ultracentrifuge with an An-50 Ti rotor (Beckman-Coulter, Brea, CA). The sedimentation coefficient distributions, corrected to standard conditions by using the SEDNTERP program (54), were calculated via least-squares boundary modeling of sedimentation velocity data using the *c*(*s*) and lsg*(*s*) methods, as implemented in the SEDFIT program (www.analyticalultracentrifugation.com)[7] (58). FTIR spectra of the different α-synuclein species (100–400 μM) were acquired in PBS and analyzed in a Bruker BioATRCell II using a Bruker Equinox 55 FTIR spectrophotometer (Bruker Optics Ltd., UK) equipped with a liquid nitrogen–cooled mercury cadmium telluride detector and a silicon internal reflection element. For each spectrum, 256 interferograms were recorded at 2 cm^{-1} resolution. Data processing of the amide I region (1720–1580 cm^{-1}) was performed with the Opus software package (Bruker Optics Ltd., UK) and consisted of a background subtraction of the buffer spectrum, atmospheric compensation, and baseline subtraction. All absorbance spectra were normalized for comparison. Far-UV CD spectra of the different α-synuclein species were acquired at 20 °C between 200 and 250 nm, using a scan speed of 50 nm min^{-1} and a bandwidth of 1 nm. 10 accumulations were recorded for each sample, using a 1-mm path length cuvette and a J-810 Jasco spectropolarimeter (Tokyo, Japan), equipped with a thermostated cell holder. The signal was converted to mean residue ellipticity. ThioT fluorescence measurements were performed in a 2 × 10-mm path length cuvette, using a Varian Cary Eclipse fluorimeter (Palo Alto, CA) in a temperature-controlled cell holder, exciting the sample at 446 nm and recording the emission fluorescence spectrum between 460 and 600 nm (5-nm slitwidths). Each protein species (10 μM) was incubated with ThioT (50 μM, 416 nm = 26,620 M^{-1} cm^{-1}) for 30 min before performing the measurement. For the seeding experiments, 10 μM of each protein species (or 5 μM in the case of the cross-seeding experiments) were added to a solution of 100 μM α-synuclein monomer, 50 μM ThioT, and 0.02% (w/v) sodium azide. The ThioT fluorescence was recorded in a BMG Fluostar Optima (BMG LABTECH, Aylesbury, Bucks, UK) using an excitation filter of 440 nm and an emission filter of 480 nm, at a constant temperature of 37 °C.

[7] Please note that the JBC is not responsible for the long-term archiving and maintenance of this site or any other third party hosted site.

Primary neurons were plated at 100,000 neurons per well in a 24-well tray onto poly-D-lysine–coated coverslips and maintained in Neurobasal media, Glutamax, and B27 as described previously. The different conformers of α-synuclein were added to neurons at 7 days *in vitro* at a final concentration of 70 nM. Neurons were fixed 7 days later, and immunofluorescence to p-α-synuclein (Abcam) and tau (Dako) was performed as described previously (4).

Internalization assay was essentially performed as described (29) with some modifications. We thus generated Alexa488-labeled fibrils and oligomers using the α-synuclein mutant E122C to incorporate the fluorophore at the upstream position of the recognized C-terminal truncation sites. E122C α-synuclein was purified and labeled using Life Technologies, Inc., Alexa488 C_5-maleimide. The labeled protein was purified from free dye using a P10 desalting column and a Sephadex G-25 matrix. To perform the internalization experiments, primary neurons were incubated for 30 min in cold PBS containing α-synuclein–Alexa488 fibrils or oligomers (final concentration 70 nM) to allow the species to bind the plasma membrane. The neurons were then transferred to 37 °C to allow internalization. Extracellular α-syn–Alexa488 fibrils were quenched with freshly made trypan blue, final concentration 1 mM in PBS. Images were captured using a Zeiss Axio Observer Z1 with Colibri LED illumination. The excitation/emission was 470/550 nm for the fibrils and 560/630 nm for trypan blue. The average intensity of each frame captured was quantified using Fiji and normalized to the fluorescence signal from trypan blue bound to the neuronal membrane.

Surgeries

Surgeries were performed using C57BL/6J mice aged 2–4 months using a digital stereotaxic frame (David Kopf). For the duration of surgery, mice were deeply anesthetized with vaporized isoflurane on a gas mask fitted to a digital stereotaxic frame. Mouse respiration was monitored throughout the procedure. Proteins for injection were drawn to a gas-tight syringe with a 26s-gauge needle (Hamilton) and controlled by a digital pump. Two μl of protein were injected, and subsequent withdrawal of the needle occurred over the course of 12 min. Solutions were injected into the right dorsal striatum using the following coordinates: 0.2 mm anterior and 2.0 mm lateral to the bregma, and 2.6 mm ventral relative to the skull. Scalp incisions were closed with EZ-Clips (Thermo Fisher Scientific).

Immunohistochemistry and immunofluorescence

Mice injected with various α-syn conformations were anesthetized post-injection with isofluorane and transcardially perfused with a saline solution (0.9% NaCl, 0.005% sodium nitroprusside, and 10 units/ml heparin sodium) followed by freshly prepared 4% paraformaldehyde (PFA) buffered in phosphate-buffered saline (PBS). Brains were removed, postfixed for 24 h in 4% PFA and PBS solution, floated into 30% sucrose PBS solution for up to 3 days, frozen in methylbutane solution (−50 °C), and stored at −80 °C. Brain tissue was sectioned at 40 μM with a freezing microtome. Immunohistochemistry and immunofluorescence were performed as described previously (55). Antibodies included the following: p-α-synuclein (EP1536Y

(Abcam)) (56); tyrosine hydroxylase (Abcam); and dopamine transporter (a generous gift from Dr. Allan Levey, Emory University) (57). For the DAT and TH immunofluorescence in the striatum, confocal images of coronal sections (bregma: −0.5 mm anterior/posterior) were captured, and ImageJ was used to quantify the integrated intensity of the dorsal portion of the striatum.

Behavior assays

All behavioral tests were performed with the help of our Neuroscience Behavioral Core, University of Alabama at Birmingham. Mice were acclimated to the test environment for at least 30 min prior to testing and were given at least a 1-day rest between each test.

Open field test—Each mouse was placed at the side of a 100 × 100 × 50-cm white Plexiglas open field. A computerized tracking system (Ethovision) recorded movement for 5 min from which we derived the following: the amount of time spent in the center of the test apparatus, and the velocity of movement.

Cylinder test—Mice were placed in a covered Plexiglas cylinder with activity recorded for 5 min by Ethovision software on a camera positioned below the cylinder. An experimenter blinded to the treatment conditions scored each video. The following behaviors were scored: number of rears, front limb steps, hind limb steps, and total steps (37).

Pole test—Mice were placed on top of a wooden pole (diameter 1 cm; height 50 cm) wrapped in chicken wire. Each subject completed five trials with a 1-min rest between each trial. Time to turn with nose facing down and time to reach the bottom of the pole were recorded and combined to derive the total time to descend. If a mouse did not climb down the pole after 2 min, the trial time was not included in that animal's average total time to descend.

Cage hang—Mice were placed on a cage top elevated 50 cm above a cage filled with bedding. The cage lid was shaken slightly and flipped over to measure latency to fall over the course of three trials (>1-min rest between each trial). A trial less than 10 s was performed again, and trials were concluded at 3 min if a mouse was still hanging.

Stereology

Stereology was completed using an Olympus BX51 microscope and StereoInvestigator software (MBF Biosciences) using the Neuroscience Molecular Detection and Stereology Core, University of Alabama at Birmingham. Contours were drawn around 6–7 serial sections containing SNc. Unbiased stereological estimation of total TH-positive neurons in the SNc contralateral and ipsilateral to injection was performed using the Optical Fractionator probe by an investigator blinded to experimental conditions.

Statistical analyses

Data were analyzed using GraphPad Prism. One-way or two-way ANOVA were performed. Outliers were identified using the ROUT method in GraphPad Prism. The only data in which two outliers were identified were in the cage hang motor test.

Author contributions—J. M. F., M. C.-C., N. M. A., J. D. C., D. R. T., A. A. Y., S. F., N. C., and L. A. V.-D. data curation; J. M. F., M. C.-C., J. F., N. M. A., J. D. C., S. W. C., J. F., S. F., J. R. K., N. C., and L. A. V.-D. formal analysis; J. R. K., N. C., and L. A. V.-D. supervision; J. M. F., M. C.-C., N. M. A., J. D. C., S. W. C., J. F., S. F., J. R. K., N. C., and L. A. V.-D. investigation; J. M. F., M. C.-C., N. M. A., J. D. C., S. W. C., D. R. T., J. F., A. A. Y., J. R. K., N. C., and L. A. V.-D. methodology; J. M. F., M. C.-C., C. M. D., N. C., and L. A. V.-D. writing-original draft; J. M. F., M. C.-C., C. M. D., J. R. K., N. C., and L. A. V.-D. writing-review and editing; N. C. and L. A. V.-D. conceptualization; N. C., and L. A. V.-D. validation; N. C. and L. A. V.-D. visualization; C. M. D., N. C., and L. A. V.-D. resources; N. C. and L. A. V.-D. software; N. C. and L. A. V.-D. funding acquisition; N. C. and L. A. V.-D. project administration.

Acknowledgments—We thank Andrew West for advice and suggestions on this work and Valentina Krendelchtchikova for help with purifying protein.

References

1. Cremades, N., and Dobson, C. M. (2018) The contribution of biophysical and structural studies of protein self-assembly to the design of therapeutic strategies for amyloid diseases. *Neurobiol. Dis.* **109,** 178–190 CrossRef Medline
2. Spillantini, M. G., Schmidt, M. L., Lee, V. M., Trojanowski, J. Q., Jakes, R., and Goedert, M. (1997) α-Synuclein in Lewy bodies. *Nature* **388,** 839–840 CrossRef Medline
3. Kuusisto, E., Parkkinen, L., and Alafuzoff, I. (2003) Morphogenesis of Lewy bodies: dissimilar incorporation of α-synuclein, ubiquitin, and p62. *J. Neuropathol. Exp. Neurol.* **62,** 1241–1253 CrossRef Medline
4. Volpicelli-Daley, L. A., Luk, K. C., Patel, T. P., Tanik, S. A., Riddle, D. M., Stieber, A., Meaney, D. F., Trojanowski, J. Q., and Lee, V. M. (2011) Exogenous α-synuclein fibrils induce Lewy body pathology leading to synaptic dysfunction and neuron death. *Neuron* **72,** 57–71 CrossRef Medline
5. Luk, K. C., Kehm, V., Carroll, J., Zhang, B., O'Brien, P., Trojanowski, J. Q., and Lee, V. M. (2012) Pathological α-synuclein transmission initiates Parkinson-like neurodegeneration in nontransgenic mice. *Science* **338,** 949–953 CrossRef Medline
6. Volpicelli-Daley, L., and Brundin, P. (2018) Prion-like propagation of pathology in Parkinson's disease. *Handb. Clin. Neurol.* **153,** 321–335 CrossRef Medline
7. Chen, S. W., Drakulic, S., Deas, E., Ouberai, M., Aprile, F. A., Arranz, R., Ness, S., Roodveldt, C., Guilliams, T., De-Genst, E. J., Klenerman, D., Wood, N. W., Knowles, T. P., Alfonso, C., Rivas, G., *et al.* (2015) Structural characterization of toxic oligomers that are kinetically trapped during α-synuclein fibril formation. *Proc. Natl. Acad. Sci. U.S.A.* **112,** E1994–E2003 CrossRef Medline
8. Bousset, L., Pieri, L., Ruiz-Arlandis, G., Gath, J., Jensen, P. H., Habenstein, B., Madiona, K., Olieric, V., Böckmann, A., Meier, B. H., and Melki, R. (2013) Structural and functional characterization of two α-synuclein strains. *Nat. Commun.* **4,** 2575 CrossRef Medline
9. Melki, R. (2018) How the shapes of seeds can influence pathology. *Neurobiol. Dis.* **109,** 201–208 CrossRef Medline
10. Dettmer, U., Newman, A. J., Soldner, F., Luth, E. S., Kim, N. C., von Saucken, V. E., Sanderson, J. B., Jaenisch, R., Bartels, T., and Selkoe, D. (2015) Parkinson-causing α-synuclein missense mutations shift native tetramers to monomers as a mechanism for disease initiation. *Nat. Commun.* **6,** 7314 CrossRef Medline
11. Burré, J., Sharma, M., and Südhof, T. C. (2014) α-Synuclein assembles into higher-order multimers upon membrane binding to promote SNARE complex formation. *Proc. Natl. Acad. Sci. U.S.A.* **111,** E4274–E4283 CrossRef Medline
12. Chandra, S., Chen, X., Rizo, J., Jahn, R., and Südhof, T. C. (2003) A broken α-helix in folded α-synuclein. *J. Biol. Chem.* **278,** 15313–15318 CrossRef Medline

13. Cremades, N., Cohen, S. I., Deas, E., Abramov, A. Y., Chen, A. Y., Orte, A., Sandal, M., Clarke, R. W., Dunne, P., Aprile, F. A., Bertoncini, C. W., Wood, N. W., Knowles, T. P., Dobson, C. M., and Klenerman, D. (2012) Direct observation of the interconversion of normal and toxic forms of α-synuclein. *Cell* **149,** 1048–1059 CrossRef Medline
14. Fusco, G., Chen, S. W., Williamson, P. T. F., Cascella, R., Perni, M., Jarvis, J. A., Cecchi, C., Vendruscolo, M., Chiti, F., Cremades, N., Ying, L., Dobson, C. M., and De Simone, A. (2017) Structural basis of membrane disruption and cellular toxicity by α-synuclein oligomers. *Science* **358,** 1440–1443 CrossRef Medline
15. Osterberg, V. R., Spinelli, K. J., Weston, L. J., Luk, K. C., Woltjer, R. L., and Unni, V. K. (2015) Progressive aggregation of α-synuclein and selective degeneration of Lewy inclusion-bearing neurons in a mouse model of parkinsonism. *Cell Rep.* **10,** 1252–1260 CrossRef Medline
16. Masuda-Suzukake, M., Nonaka, T., Hosokawa, M., Kubo, M., Shimozawa, A., Akiyama, H., and Hasegawa, M. (2014) Pathological α-synuclein propagates through neural networks. *Acta Neuropathol. Commun.* **2,** 88 CrossRef Medline
17. Abdelmotilib, H., Maltbie, T., Delic, V., Liu, Z., Hu, X., Fraser, K. B., Moehle, M. S., Stoyka, L., Anabtawi, N., Krendelchtchikova, V., Volpicelli-Daley, L. A., and West, A. (2017) α-Synuclein fibril-induced inclusion spread in rats and mice correlates with dopaminergic neurodegeneration. *Neurobiol. Dis.* **105,** 84–98 CrossRef Medline
18. Tarutani, A., Suzuki, G., Shimozawa, A., Nonaka, T., Akiyama, H., Hisanaga, S., and Hasegawa, M. (2016) The effect of fragmented pathogenic α-synuclein seeds on prion-like propagation. *J. Biol. Chem.* **291,** 18675–18688 CrossRef Medline
19. Polinski, N. K., Volpicelli-Daley, L. A., Sortwell, C. E., Luk, K. C., Cremades, N., Gottler, L. M., Froula, J., Duffy, M. F., Lee, V. M. Y., Martinez, T. N., and Dave, K. D. (2018) Best practices for generating and using α-synuclein pre-formed fibrils to model Parkinson's disease in rodents. *J. Parkinsons Dis.* **8,** 303–322 CrossRef Medline
20. Luk, K. C., Covell, D. J., Kehm, V. M., Zhang, B., Song, I. Y., Byrne, M. D., Pitkin, R. M., Decker, S. C., Trojanowski, J. Q., and Lee, V. M. (2016) Molecular and biological compatibility with host α-synuclein influences fibril pathogenicity. *Cell Rep.* **16,** 3373–3387 CrossRef Medline
21. Xu, G., Gonzales, V., and Borchelt, D. R. (2002) Rapid detection of protein aggregates in the brains of Alzheimer patients and transgenic mouse models of amyloidosis. *Alzheimer Dis. Assoc. Disord.* **16,** 191–195 CrossRef Medline
22. Chang, E., and Kuret, J. (2008) Detection and quantification of τ aggregation using a membrane filter assay. *Anal. Biochem.* **373,** 330–336 CrossRef Medline
23. Celej, M. S., Sarroukh, R., Goormaghtigh, E., Fidelio, G. D., Ruysschaert, J. M., and Raussens, V. (2012) Toxic prefibrillar α-synuclein amyloid oligomers adopt a distinctive antiparallel β-sheet structure. *Biochem. J.* **443,** 719–726 CrossRef Medline
24. Cerf, E., Sarroukh, R., Tamamizu-Kato, S., Breydo, L., Derclaye, S., Dufrêne, Y. F., Narayanaswami, V., Goormaghtigh, E., Ruysschaert, J. M., and Raussens, V. (2009) Antiparallel β-sheet: a signature structure of the oligomeric amyloid β-peptide. *Biochem. J.* **421,** 415–423 CrossRef Medline
25. Qiang, W., Yau, W. M., Luo, Y., Mattson, M. P., and Tycko, R. (2012) Antiparallel β-sheet architecture in Iowa-mutant β-amyloid fibrils. *Proc. Natl. Acad. Sci. U.S.A.* **109,** 4443–4448 CrossRef Medline
26. Kayed, R., Canto, I., Breydo, L., Rasool, S., Lukacsovich, T., Wu, J., Albay R., 3rd., Pensalfini, A., Yeung, S., Head, E., Marsh, J. L., and Glabe, C. (2010) Conformation dependent monoclonal antibodies distinguish different replicating strains or conformers of prefibrillar Aβ oligomers. *Mol. Neurodegener.* **5,** 57 CrossRef Medline
27. Kayed, R., Head, E., Thompson, J. L., McIntire, T. M., Milton, S. C., Cotman, C. W., and Glabe, C. G. (2003) Common structure of soluble amyloid oligomers implies common mechanism of pathogenesis. *Science* **300,** 486–489 CrossRef Medline
28. Fujiwara, H., Hasegawa, M., Dohmae, N., Kawashima, A., Masliah, E., Goldberg, M. S., Shen, J., Takio, K., and Iwatsubo, T. (2002) α-Synuclein is phosphorylated in synucleinopathy lesions. *Nat. Cell Biol.* **4,** 160–164 CrossRef Medline
29. Karpowicz, R. J., Jr., Haney, C. M., Mihaila, T. S., Sandler, R. M., Petersson, E. J., and Lee, V. M. (2017) Selective imaging of internalized proteopathic α-synuclein seeds in primary neurons reveals mechanistic insight into transmission of synucleinopathies. *J. Biol. Chem.* **292,** 13482–13497 CrossRef Medline
30. Paumier, K. L., Luk, K. C., Manfredsson, F. P., Kanaan, N. M., Lipton, J. W., Collier, T. J., Steece-Collier, K., Kemp, C. J., Celano, S., Schulz, E., Sandoval, I. M., Fleming, S., Dirr, E., Polinski, N. K., Trojanowski, J. Q., *et al.* (2015) Intrastriatal injection of pre-formed mouse α-synuclein fibrils into rats triggers α-synuclein pathology and bilateral nigrostriatal degeneration. *Neurobiol. Dis.* **82,** 185–199 CrossRef Medline
31. Rey, N. L., Steiner, J. A., Maroof, N., Luk, K. C., Madaj, Z., Trojanowski, J. Q., Lee, V. M., and Brundin, P. (2016) Widespread transneuronal propagation of α-synucleinopathy triggered in olfactory bulb mimics prodromal Parkinson's disease. *J. Exp. Med.* **213,** 1759–1778 CrossRef Medline
32. Masuda-Suzukake, M., Nonaka, T., Hosokawa, M., Oikawa, T., Arai, T., Akiyama, H., Mann, D. M., and Hasegawa, M. (2013) Prion-like spreading of pathological α-synuclein in brain. *Brain* **136,** 1128–1138 CrossRef Medline
33. Popova, B., Kleinknecht, A., and Braus, G. H. (2015) Posttranslational modifications and clearing of α-synuclein aggregates in yeast. *Biomolecules* **5,** 617–634 CrossRef Medline
34. Pan, W. X., Mao, T., and Dudman, J. T. (2010) Inputs to the dorsal striatum of the mouse reflect the parallel circuit architecture of the forebrain. *Front. Neuroanat.* **4,** 147 CrossRef Medline
35. Vargas, K. J., Schrod, N., Davis, T., Fernandez-Busnadiego, R., Taguchi, Y. V., Laugks, U., Lucic, V., and Chandra, S. S. (2017) Synucleins have multiple effects on presynaptic architecture. *Cell Rep.* **18,** 161–173 CrossRef Medline
36. Ogawa, N., Hirose, Y., Ohara, S., Ono, T., and Watanabe, Y. (1985) A simple quantitative bradykinesia test in MPTP-treated mice. *Res. Commun. Chem. Pathol. Pharmacol.* **50,** 435–441 Medline
37. Dirr, E. R., Ekhator, O. R., Blackwood, R., Holden, J. G., Masliah, E., Schultheis, P. J., and Fleming, S. M. (2018) Exacerbation of sensorimotor dysfunction in mice deficient in Atp13a2 and overexpressing human wildtype α-synuclein. *Behav. Brain Res.* **343,** 41–49 CrossRef Medline
38. Deas, E., Cremades, N., Angelova, P. R., Ludtmann, M. H., Yao, Z., Chen, S., Horrocks, M. H., Banushi, B., Little, D., Devine, M. J., Gissen, P., Klenerman, D., Dobson, C. M., Wood, N. W., Gandhi, S., and Abramov, A. Y. (2016) α-Synuclein oligomers interact with metal ions to induce oxidative stress and neuronal death in Parkinson's disease. *Antioxid. Redox Signal.* **24,** 376–391 CrossRef Medline
39. Angelova, P. R., Ludtmann, M. H., Horrocks, M. H., Negoda, A., Cremades, N., Klenerman, D., Dobson, C. M., Wood, N. W., Pavlov, E. V., Gandhi, S., and Abramov, A. Y. (2016) Ca^{2+} is a key factor in α-synuclein–induced neurotoxicity. *J. Cell Sci.* **129,** 1792–1801 CrossRef Medline
40. Gao, X., Carroni, M., Nussbaum-Krammer, C., Mogk, A., Nillegoda, N. B., Szlachcic, A., Guilbride, D. L., Saibil, H. R., Mayer, M. P., and Bukau, B. (2015) Human Hsp70 disaggregase reverses Parkinson's-linked α-synuclein amyloid fibrils. *Mol. Cell* **59,** 781–793 CrossRef Medline
41. Abeliovich, A., Schmitz, Y., Fariñas, I., Choi-Lundberg, D., Ho, W. H., Castillo, P. E., Shinsky, N., Verdugo, J. M., Armanini, M., Ryan, A., Hynes, M., Phillips, H., Sulzer, D., and Rosenthal, A. (2000) Mice lacking α-synuclein display functional deficits in the nigrostriatal dopamine system. *Neuron* **25,** 239–252 CrossRef Medline
42. Zharikov, A. D., Cannon, J. R., Tapias, V., Bai, Q., Horowitz, M. P., Shah, V., El Ayadi, A., Hastings, T. G., Greenamyre, J. T., and Burton, E. A. (2015) shRNA targeting α-synuclein prevents neurodegeneration in a Parkinson's disease model. *J. Clin. Invest.* **125,** 2721–2735 CrossRef Medline
43. Weihofen, A., Liu, Y., Arndt, J. W., Huy, C., Quan, C., Smith, B. A., Baeriswyl, J. L., Cavegn, N., Senn, L., Su, L., Marsh, G., Auluck, P. K., Montrasio, F., Nitsch, R. M., Hirst, W. D., *et al.* (2019) Development of an aggregate-selective, human-derived α-synuclein antibody BIIB054 that ameliorates disease phenotypes in Parkinson's disease models. *Neurobiol. Dis.* **124,** 276–288 CrossRef Medline
44. Winner, B., Jappelli, R., Maji, S. K., Desplats, P. A., Boyer, L., Aigner, S., Hetzer, C., Loher, T., Vilar, M., Campioni, S., Tzitzilonis, C., Soragni, A.,

Jessberger, S., Mira, H., Consiglio, A., *et al.* (2011) *In vivo* demonstration that α-synuclein oligomers are toxic. *Proc. Natl. Acad. Sci. U.S.A.* **108,** 4194–4199 CrossRef Medline

45. Di Maio, R., Barrett, P. J., Hoffman, E. K., Barrett, C. W., Zharikov, A., Borah, A., Hu, X., McCoy, J., Chu, C. T., Burton, E. A., Hastings, T. G., and Greenamyre, J. T. (2016) α-Synuclein binds to TOM20 and inhibits mitochondrial protein import in Parkinson's disease. *Sci. Transl. Med.* **8,** 342ra78 CrossRef Medline
46. Mor, D. E., Tsika, E., Mazzulli, J. R., Gould, N. S., Kim, H., Daniels, M. J., Doshi, S., Gupta, P., Grossman, J. L., Tan, V. X., Kalb, R. G., Caldwell, K. A., Caldwell, G. A., Wolfe, J. H., and Ischiropoulos, H. (2017) Dopamine induces soluble α-synuclein oligomers and nigrostriatal degeneration. *Nat. Neurosci.* **20,** 1560–1568 CrossRef Medline
47. Holmes, B. B., DeVos, S. L., Kfoury, N., Li, M., Jacks, R., Yanamandra, K., Ouidja, M. O., Brodsky, F. M., Marasa, J., Bagchi, D. P., Kotzbauer, P. T., Miller, T. M., Papy-Garcia, D., and Diamond, M. I. (2013) Heparan sulfate proteoglycans mediate internalization and propagation of specific proteopathic seeds. *Proc. Natl. Acad. Sci. U.S.A.* **110,** E3138–E3147 CrossRef Medline
48. Mao, X., Ou, M. T., Karuppagounder, S. S., Kam, T. I., Yin, X., Xiong, Y., Ge, P., Umanah, G. E., Brahmachari, S., Shin, J. H., Kang, H. C., Zhang, J., Xu, J., Chen, R., Park, H., *et al.* (2016) Pathological α-synuclein transmission initiated by binding lymphocyte-activation gene 3. *Science* **353,** aah3374 CrossRef Medline
49. Shrivastava, A. N., Redeker, V., Fritz, N., Pieri, L., Almeida, L. G., Spolidoro, M., Liebmann, T., Bousset, L., Renner, M., Léna, C., Aperia, A., Melki, R., and Triller, A. (2015) α-Synuclein assemblies sequester neuronal α3-Na^+/K^+-ATPase and impair Na^+ gradient. *EMBO J.* **34,** 2408–2423 CrossRef Medline
50. Luk, K. C., Kehm, V. M., Zhang, B., O'Brien, P., Trojanowski, J. Q., and Lee, V. M. (2012) Intracerebral inoculation of pathological α-synuclein initiates a rapidly progressive neurodegenerative α-synucleinopathy in mice. *J. Exp. Med.* **209,** 975–986 CrossRef Medline
51. Prusiner, S. B., Woerman, A. L., Mordes, D. A., Watts, J. C., Rampersaud, R., Berry, D. B., Patel, S., Oehler, A., Lowe, J. K., Kravitz, S. N., Geschwind, D. H., Glidden, D. V., Halliday, G. M., Middleton, L. T., Gentleman, S. M., *et al.* (2015) Evidence for α-synuclein prions causing multiple system atrophy in humans with parkinsonism. *Proc. Natl. Acad. Sci. U.S.A.* **112,** E5308–E5317 CrossRef Medline
52. Peng, C., Gathagan, R. J., Covell, D. J., Medellin, C., Stieber, A., Robinson, J. L., Zhang, B., Pitkin, R. M., Olufemi, M. F., Luk, K. C., Trojanowski, J. Q., and Lee, V. M. (2018) Cellular milieu imparts distinct pathological α-synuclein strains in α-synucleinopathies. *Nature* **557,** 558–563 CrossRef Medline
53. Volpicelli-Daley, L. A., Luk, K. C., and Lee, V. M. (2014) Addition of exogenous α-synuclein preformed fibrils to primary neuronal cultures to seed recruitment of endogenous α-synuclein to Lewy body and Lewy neurite-like aggregates. *Nat. Protoc.* **9,** 2135–2146 CrossRef Medline
54. Laue, T. M., Shah, B. D., Ridgeway, T. M., and Pelletier, S. L. (1992) in *Analytical Ultracentrifugation in Biochemistry and Polymer Science* (Harding, S. E., Rowe, A. J., and Horton, J. C., eds) pp. 90–125, The Royal Society of Chemistry, Cambridge, UK
55. Volpicelli-Daley, L. A., and Levey, A. (2004) Immunohistochemical localization of proteins in the nervous system. *Curr. Protoc. Neurosci.* 2004 Chapter 1, Unit 1.2 CrossRef Medline
56. Rutherford, N. J., Brooks, M., and Giasson, B. I. (2016) Novel antibodies to phosphorylated α-synuclein serine 129 and NFL serine 473 demonstrate the close molecular homology of these epitopes. *Acta Neuropathol. Commun.* **4,** 80 CrossRef Medline
57. Hersch, S. M., Yi, H., Heilman, C. J., Edwards, R. H., and Levey, A. I. (1997) Subcellular localization and molecular topology of the dopamine transporter in the striatum and substantia nigra. *J. Comp. Neurol.* **388,** 211–227 CrossRef Medline
58. Schuck, P. (2000) Size-distribution analysis of macromolecules by sedimentation velocity ultracentrifugation and lamm equation modeling. *Biophys. J.* **78,** 1606–1619 CrossRef Medline